RSC Advances

PAPER

View Article Online
View Journal | View Issue

Cite this: *RSC Adv.*, 2024, **14**, 39373

Comparative optical thermometry analysis using $Na_2SrP_2O_7:Er^{3+}/Yb^{3+}$ phosphors: evaluation of LIR_{TCL} and LIR_{NTCL} methods for high-resolution temperature sensing

Mouna Fhoula,[a] Mohamed Khitouni[bc] and Mohamed Dammak *[a]

Optical thermometry is a valuable non-contact technique for temperature measurement, especially in environments where traditional methods are impractical. Despite its advantages, enhancing the precision of optical thermometers remains a significant challenge. In this study, we explored the thermometric properties of $Na_2SrP_2O_7$ phosphors co-doped with Er^{3+}/Yb^{3+}, synthesized *via* a solid-state reaction method, for temperature sensing within the 200–440 K range under 980 nm excitation. Upconversion (UC) luminescence, observed in the visible spectrum, was analyzed using the fluorescence intensity ratio (FIR) method, focusing on both thermally coupled (TCLs) and non-thermally coupled (NTCLs) energy levels of Er^{3+}/Yb^{3+}. Specifically, the transitions $^2H_{11/2} \rightarrow {}^4I_{15/2}$, $^4S_{3/2} \rightarrow {}^4I_{15/2}$, and $^4F_{9/2} \rightarrow {}^4I_{15/2}$ were examined to calculate thermometric parameters. The maximum absolute sensitivity (S_A) and relative sensitivity (S_R) for the $^2H_{11/2} \rightarrow {}^4I_{15/2}$ to $^4S_{3/2} \rightarrow {}^4I_{15/2}$ transition were 0.0009 K^{-1} and 0.6% K^{-1}, respectively, while for the $^2H_{11/2} \rightarrow {}^4I_{15/2}$ to $^4F_{9/2} \rightarrow {}^4I_{15/2}$ transition, S_A was 0.004 K^{-1}, with a maximum S_R of 1.14% K^{-1}. Furthermore, by employing a luminescence intensity ratio technique based on TCLs (LIR_{TCL}), the minimum temperature uncertainty (δT) was found to be 1.31 K at 320 K. In contrast, the luminescence intensity ratio method based on NTCLs (LIR_{NTCL}) yielded a much lower minimum δT value of 0.34 K at 200 K, indicating superior performance in terms of temperature resolution. These findings demonstrate that the LIR_{NTCL} technique provides more sensitive and accurate temperature measurement compared to LIR_{TCL}. The excellent temperature resolution and sensitivity of $Na_2SrP_2O_7:Er^{3+}/Yb^{3+}$ phosphors highlight their potential for highly accurate optical thermometry applications in scientific and industrial contexts.

Received 4th November 2024
Accepted 2nd December 2024

DOI: 10.1039/d4ra07853e

rsc.li/rsc-advances

1. Introduction

Temperature, as an important physical parameter, has significant impacts on many physical, chemical, and biological processes.[1,2] Traditional temperature measuring devices, such as thermometers and thermocouples, which are limited by response time and spatial resolution, are no longer applicable. In the last few years, non-contact sensing techniques have attracted great attention. These new technologies exhibit some advantages, such as remote operation, safety and high sensitivity.[3–5] Among the non-contact temperature sensing technologies, luminescence thermometry has attracted significant attention because of its advantages of rapid response capability, non-invasive operation and high-spatial resolution.[6–8] Essentially, there are three commonly used techniques for temperature sensing using thermographic phosphors: the peak intensity ratio, lifetime and rise time of luminescence. Indeed, the luminescence intensity ratio (LIR) is the most commonly used temperature sensing method. The LIR is determined by measuring optical emission intensity variations from thermally coupled transitions at different temperatures. LIR technology is based on changes in emission intensity ratios caused by temperature variations. These ratios can either reflect the interaction between two thermally coupled levels of a single lanthanide ion or emissions from several different lanthanide ions.[9–11] Generally, the presence of two closely spaced states with a gap smaller than 2000 cm^{-1} is considered the condition for thermal coupling of transitions to occur. In this case, the LIR curve is typically fitted if both the states share the electronic population according to Boltzmann distribution.[12] However, because of the small energy gap and spectral overlapping, TCL-based optical thermometers suffer from low sensitivity and a narrow temperature range, limiting their

[a]*Laboratoire de Physique Appliquée, Groupe des Matériaux Luminescents, Faculté des Sciences de Sfax, Département de Physique, Université de Sfax, Sfax B.P. 3000, Tunisia. E-mail: madidammak@yahoo.fr; Mohamed.dammak@fss.usf.tn*

[b]*Department of Chemistry, College of Science, Qassim University, Buraidah 51452, Saudi Arabia*

[c]*Laboratory of Inorganic Chemistry, LR17-ES-07, Faculty of Science, University of Sfax, Sfax 3018, Tunisia*

practical use.[13,14] LIR methods based on non-thermally coupled levels (NTCLs) can be used to avoid the above problems because the emission bands of two luminescent center ions do not overlap. Thus, the discovery of alternative luminescent materials suitable for temperature sensing is an important goal to achieve optical thermometry that operates over a wide temperature range with high sensitivity using the LIR of NTCLs.[15,16]

Luminescence centers and host matrixes are two significant factors for efficient UC emission, which is widely used for optical temperature measurement. Rare-earth (RE) ions are considered the best candidates for luminescence centers owing to their abundant energy levels and high conversion efficiency. Different RE ions have been studied for temperature sensing, such as Er^{3+}, Tm^{3+}, Dy^{3+}, Ho^{3+}, and Nd^{3+}.[17] From these, Er^{3+} is one of the most efficient activators because of its strong green up-conversion luminescence. Nevertheless, an Er^{3+} ion single-doped phosphor material exhibits low up-conversion efficiency due to its small absorption cross section. Simultaneously, to enhance green emission intensity, Yb^{3+} can be used as a sensitizer for its large absorption cross section over the near-infrared region. Yb^{3+} is also able to transport its energy to the activator ion *via* an excited-state absorption route. Thus, co-doping Yb^{3+} and Er^{3+} has become the preferred rare earth combination in temperature-sensitive application.[18–25]

Active research is highly sought after to develop new inorganic phosphor materials with better temperature-sensing properties. Currently, phosphates are widely used as host materials considering their high emission efficiency; excellent thermal, mechanical and chemical stability; and better color rendering index. These properties make them ideal for a wide range of display devices and highlight their potential for use in white light-emitting diodes (WLEDs).[26] Different phosphors derived from inorganic phosphates have been investigated as effective luminescence materials for displays[27–29] and optical thermometry.[18,30–32] To date, the UC luminescence properties and optical thermometry of Er^{3+}/Yb^{3+} co-doped $Na_2SrP_2O_7$ have never been investigated.

In the present paper, an $Na_2SrP_2O_7$ (NSPO) host matrix co-doped with Er^{3+}/Yb^{3+} were prepared *via* the solid-state reaction method. The dependency of Yb^{3+} concentration and laser power on the UC luminescence characteristics of Er^{3+} and Yb^{3+} ions under 980 nm excitation were studied. The energy transfer mechanisms between Yb^{3+} and Er^{3+} ions were also investigated. Moreover, LIR thermometry based on TCLs and NTCLs of the nanorods was analyzed.

2. Experimental

2.1. Sample preparation

The pyrophosphate $Na_2SrP_2O_7$:2%Er^{3+},*x*%Yb^{3+} ($x = 3$, 5, 10, and 15% mol) was prepared using the conventional solid-state reaction method. This involved mixing sodium carbonate (Na_2CO_3), strontium carbonate ($SrCO_3$), di-ammonium hydrogen phosphate $(NH_4)_2HPO_4$, erbium oxide (Er_2O_3), and ytterbium oxide (Yb_2O_3). Initially, the mixtures were carefully ground together into fine powder with an agate mortar and then progressively heated up to 300 °C to evacuate ammonia and water. The resulting powders were shaped into cylindrical pellets to promote condensation. The samples were then sintered at 700 °C for 12 h in an air atmosphere with a heating rate of 5 °C min^{-1} before cooling down to room temperature.

2.2. Characterization tools

XRD measurements were performed in grazing incidence using SIEMENS -D8-$\theta/2\theta$ with a Cu Kα X-ray source ($\lambda = 0.15418$ nm) at glancing angles between 10° and 70°. The Fourier transform infrared (FT-IR) spectrum for the title compound was recorded at room temperature on a PerkinElmer Spectrum 1000 FT-IR spectrometer in the range 400–4000 cm^{-1}. UC emission spectra were carefully analyzed using a PerkinElmer Lambda

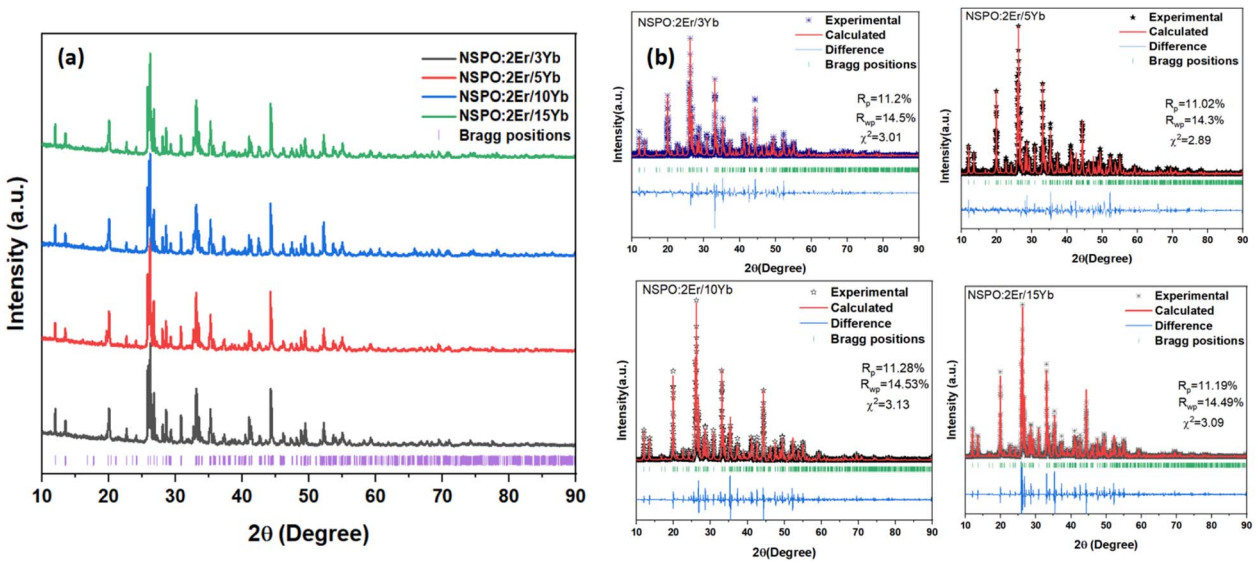

Fig. 1 (a) X-ray powder diffraction patterns and (b) XRD Rietveld refinements of NSPO:2%Er,*x*%Yb ($x = 3$, 5, 10, and 15).

365 spectrometer. For the dependent temperature, the sample was placed in a cryostat, and its photoluminescence (PL) spectra were measured with a Horiba-Jobin Yvon HR 320 spectrometer with a 980 nm laser excitation source.

3. Results and discussion

3.1. X-ray diffraction study

The X-ray diffraction patterns of NSPO:2%Er,*x*%Yb ($x = 3$, 5, 10, and 15) are shown in Fig. 1a. The intensity and position of the diffraction peaks of the four samples are almost the same. In order to verify phase purity, the Rietveld refinement XRD patterns of different samples were obtained using Rietveld refinement (Fig. 1b). There are no impurity peaks between the experimental patterns and the calculated data. The refinement results reveal that the NSPO:Er,Yb compound crystallizes in the orthorhombic system with the *Pnma* space group, and lattice parameters presented in Table 1 are in agreement with those reported in the literature.[33]

3.2. FTIR studies

Fig. 2 shows the infrared spectrum of the NSPO:2%Er,15%Yb sample recorded at room temperature in the range of 1400–400 cm^{-1}. Band assignments were obtained by comparing the observed peaks with those of similar compounds reported in the literature.[33,34] The primary vibrational modes in the spectrum are attributed to the internal modes of the P_2O_7 group, particularly the characteristic vibrations of PO_3 groups and P–O–P bridging bonds.

Table 1 Unit cell parameters of NSPO:2%Er,*x*%Yb

x	*a* (Å)	*b* (Å)	*c* (Å)	*V* (Å^3)
3	8.908	5.408	13.092	630.714
5	8.917	5.414	13.104	632.672
10	8.918	5.406	13.009	631.358
15	8.919	5.401	13.117	631.819

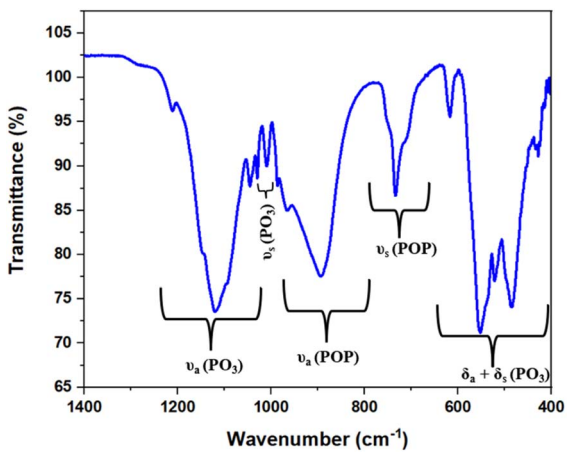

Fig. 2 FTIR spectrum of NSPO:2%Er,15%Yb.

Specifically, bands in the range 1212–1008 cm^{-1} were tentatively assigned to the symmetric and antisymmetric stretching modes of the PO_3 group, which are typical of the phosphate network. Bands in the region 984–731 cm^{-1} are associated with the symmetric and antisymmetric stretching modes of P–O–P bridges (POP), reflecting the connectivity within the phosphate structure. The absorption bands in the lower frequency range of 618–425 cm^{-1} are attributed to the symmetric and antisymmetric deformation modes, $\delta(PO_3)$, which are associated with bending vibrations of PO_3 groups.

3.3. Upconversion emission studies

Fig. 3 shows the UC emission spectra of 2%Er^{3+},*x*%Yb^{3+} co-doped NSPO particles excited at 980 nm. The spectra exhibit the typical transitions of Er^{3+} ions: two intense green bands located at 523 nm and 544 nm are assigned to the $^2H_{11/2} \rightarrow {}^4I_{15/2}$ (band H) and $^4S_{3/2} \rightarrow {}^4I_{15/2}$ (band S) transitions, respectively, while the red band corresponds to the $^4F_{9/2} \rightarrow {}^4I_{15/2}$ (band F) transition at 662 nm.[18,35] As Yb^{3+} concentration increases, a great enhancement in Er^{3+} emission is observed, which is attributed to the improved absorption by Yb^{3+} at 980 nm. This suggests that Yb^{3+} ions function as sensitizers for Er^{3+} through energy transfer from Yb^{3+} to Er^{3+}.[36]

The dependence of emission intensity on pump power is recorded to investigate the UC emission mechanism. Fig. 4 shows such a plot of the integral emission intensity (I) of the green and red emission lines as a function of pump laser power (P). In the upconversion process, the relationship between I and P can be written as:[37] $I \propto P^n$. Where n is the number of pump photons absorbed for each upconverted visible photon emitted. The slope values obtained for the two green bands (H and S) and the red band (F) are 2.25, 1.76, and 1.54, respectively. These values of n approximate to 2, revealing that UC emissions in the NSPO:Er/Yb sample come from two-photon processes.

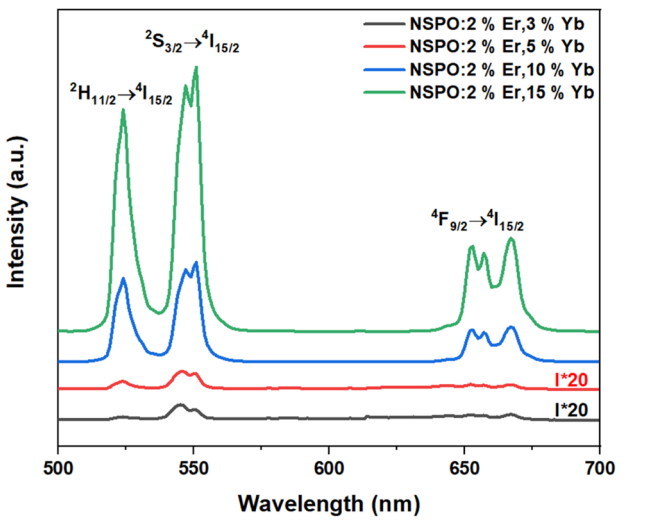

Fig. 3 UC emission spectra of NSPO:2%Er^{3+},*x*%Yb^{3+} ($x = 3$, 5, 10, and 15) under excitation at 980 nm.

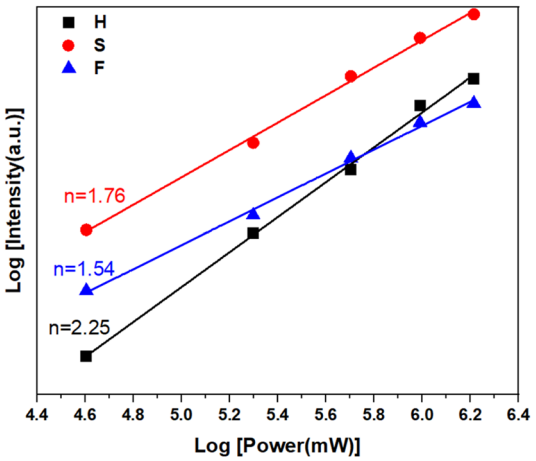

Fig. 4 Log–log plots of up-conversion emission intensity *versus* pump power for NSPO:2%Er,15%Yb under 980 nm laser excitation.

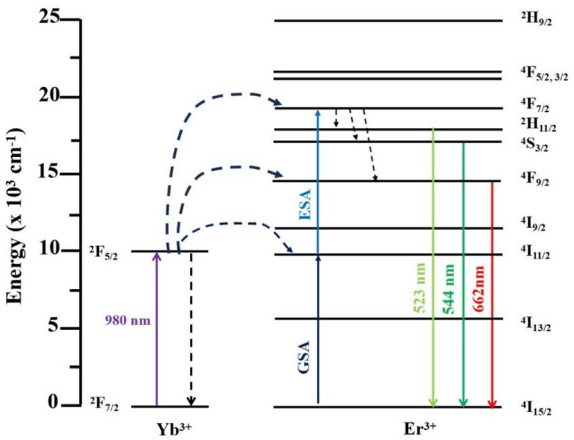

Fig. 5 Energy level diagrams of Er^{3+} and Yb^{3+} ions and the possible UC mechanisms.

To further explain the UC process between Er^{3+} and Yb^{3+}, the luminescence mechanism and possible energy transfer level diagram were drawn, as shown in Fig. 5. Under 980 nm laser excitation, the $^4I_{11/2}$ energy level of Er^{3+} ions gets populated through the ground state absorption (GSA) method by absorbing energy from Yb^{3+} ions. Subsequently, by the excited state absorption (ESA) process, the $^4F_{7/2}$ level is populated through absorption of another photon of the same energy. Photons in the $^4F_{7/2}$ level non-radiatively relax to the $^2H_{11/2}$ and $^4S_{3/2}$ states. Meanwhile, the $^2H_{11/2}$ and $^4S_{3/2}$ levels relax back to the ground emitting green light at around 523 nm and 544 nm. Finally, the Er^{3+} in the $^4F_{9/2}$ level transfers to the $^4I_{15/2}$ level, resulting in a red emission centered at 662 nm. Owing to the larger absorption cross section of Yb^{3+} and the high matching energy levels between Yb^{3+} and Er^{3+} ions, the energy transfer processes mentioned above are very efficient, resulting in intensive UC emission.[22,38,39]

3.4. Optical temperature sensing based on TCLs and NTCLs

To explore the probability of thermometry application, temperature dependent UC emission spectra under 980 nm laser excitation in the range of 200–440 K were plotted, as shown in Fig. 6a. It is clearly observed in Fig. 6b that the intensity of the $^2H_{11/2} \rightarrow {}^4I_{15/2}$ transition increases and the intensities of both $^4S_{3/2} \rightarrow {}^4I_{15/2}$ and $^4F_{9/2} \rightarrow {}^4I_{15/2}$ transitions decrease gradually with increasing temperatures, while the shape and position of the emission peaks remain unchanged. Thus, the different change tendencies of emission intensities can be used to achieve greater sensing thermometry. For thermally coupled energy levels, the luminescence intensity ratio (LIR_{TCL}) is governed by the Boltzmann distribution law and can be expressed as follows:[40–43]

$$LIR_{TCL} = \frac{I_H}{I_S} = A\exp\left(-\frac{\Delta E}{k_B T}\right) + C = A\exp\left(-\frac{B}{T}\right) + C \quad (1)$$

where I_H and I_S are the integrated intensities of green emissions corresponding to the transitions $^2H_{11/2} \rightarrow {}^4I_{15/2}$ and $^4S_{3/2} \rightarrow {}^4I_{15/2}$, respectively. B is a pre-exponential constant, ΔE is the thermal coupling energy level difference, k_B is the Boltzmann constant, T is the absolute temperature, and C is a constant.

Fig. 7a shows the temperature-dependent LIR_{TCL} for NSPO:Er,Yb. As can be observed, the LIR_{TCL} increases as the

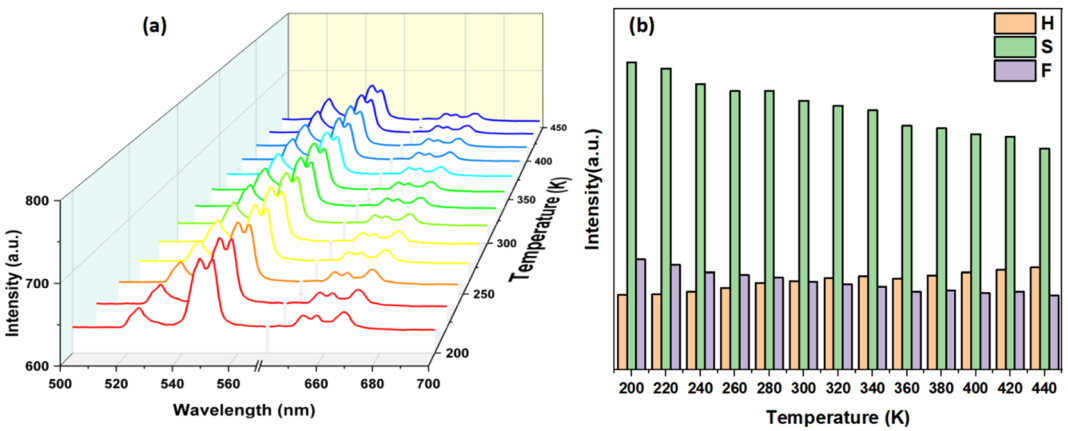

Fig. 6 (a) UC emission spectra of NSPO:2%Er,15%Yb under 980 nm laser excitation in the 200–440 K temperature range, and (b) histograms of the temperature-dependent integral PL intensities of bands H, S, and F.

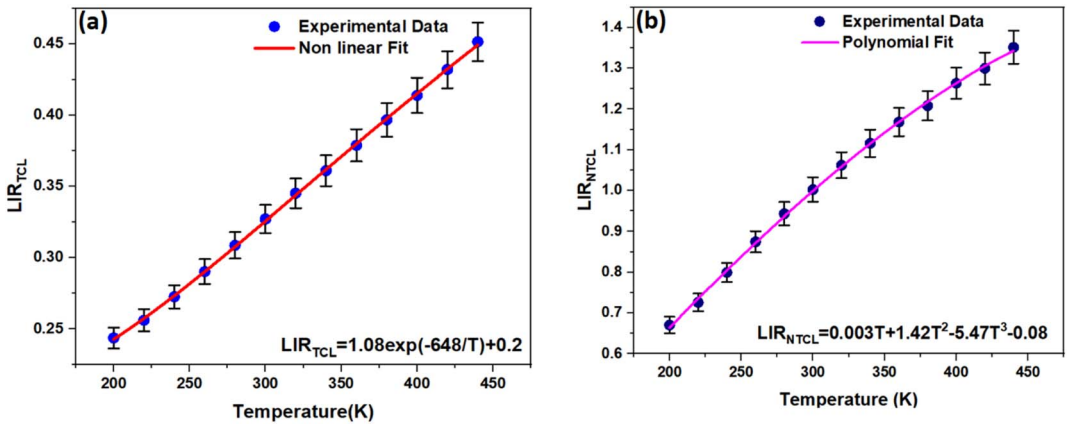

Fig. 7 (a) LIR_{TCL} and (b) LIR_{NTCL} values as a function of temperature. The error bars indicate uncertainties due to experimental acquisition and data analysis.

temperature increases, in alignment with the fit curve described in eqn (1), in which the fitting function is $LIR_{TCL} = 1.08 \exp(-648.8/T) + 0.2$ with $R^2 = 0.999$, indicating a good fit. Next, the energy gap between $^2H_{11/2}$ and $^4S_{3/2}$ levels was calculated to be approximately 450 cm^{-1}.

Moreover, noncontact optical temperature sensing using the LIR of NTCLs is investigated to improve sensing sensitivity. Fig. 7b exhibits the temperature-dependent UC LIR_{NTCL} of the other pair associated to NTCL: $^2H_{11/2} \rightarrow {}^4I_{15/2}$ and $^4F_{9/2} \rightarrow {}^4I_{15/2}$ in the temperature range of 200–440 K. It is rare for NTCLs to be affected by thermal excitation because of their large energy gaps, which makes the traditional LIR method unsuitable.[44] Therefore, the experimental data could be typically fitted in alignment with the following polynomial expression:

$$LIR_{NTCL} = \frac{I_H}{I_F} = B_0 + B_1 T + B_2 T^2 + B_3 T^3 \quad (2)$$

where B_1, B_2, and B_3 represent thermometry constants. The fitting formula obtained from Fig. 7b is $LIR_{NTCL} = -0.08 + 0.003T + 1.42T^2 - 5.47T^3$ and $R^2 = 0.993$, indicating that the fit is good.

In addition, the sensitivity of the sensor is a key indicator for actual optical temperature measurement. Two sensitivity parameters are defined: absolute sensitivity S_A, which indicates the rate of change in the LIR with temperature, and relative sensitivity S_R, which represents the relative variation in LIR with unit temperature. These parameters can be expressed by the following equations:[36,39,45]

$$S_A = \frac{\partial LIR}{\partial T}$$

$$S_R = \frac{1}{LIR} \times \frac{\partial LIR}{\partial T} \times 100\%$$

Fig. 8 depicts the evolution of S_A and S_R values in the temperature range of 200–440 K. Firstly, S_A values based on LIR_{NTCL} are much larger than those based on LIR_{TCL} in the whole experimental temperature range. As it can be noticed, the maximum values of S_A were found to be 0.0018 K^{-1} at 320 K and 0.0075 K^{-1} at 200 K for LIR_{TCL} and LIR_{NTCL}, respectively. Secondly, the maximum value of S_R obtained using LIR_{TCL} was 0.6% K^{-1} at 240 K, while that obtained using LIR_{NTCL} kept

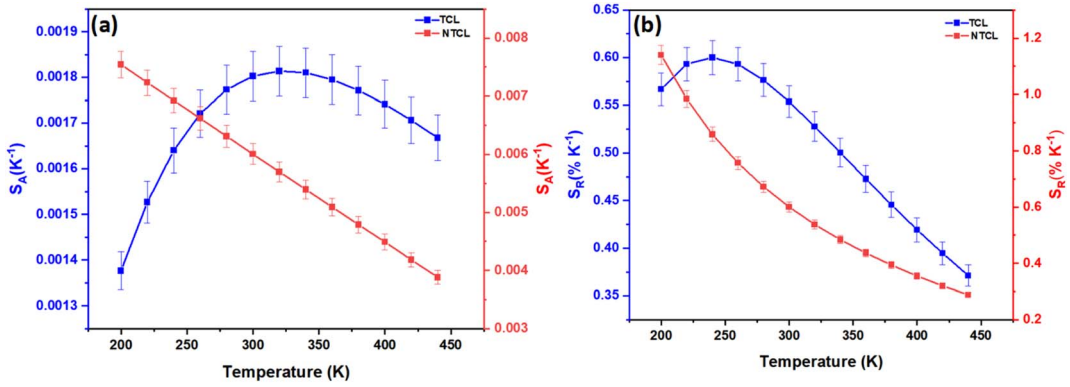

Fig. 8 (a) Absolute sensitivity and (b) relative sensitivity of thermally and non-thermally coupled levels as a function of temperature from 200 K to 440 K. The error bars indicate uncertainties due to experimental acquisition and data analysis.

Table 2 Maximum relative sensitivity of Er^{3+}, Yb^{3+} based luminescent thermometers using thermally and non-thermally coupled levels

System	T range (K)	LIR	S_A (K^{-1})	S_R (% K^{-1})	Ref.
$NaSrPO_4$:Er/Yb	298–573	$^2H_{11/2} \rightarrow {}^4I_{15/2}/{}^4S_{3/2} \rightarrow {}^4I_{15/2}$	0.0052	1.78 (298 K)	18
$NaZnPO_4$:Er/Yb	303–753	$^2H_{11/2} \rightarrow {}^4I_{15/2}/{}^4S_{3/2} \rightarrow {}^4I_{15/2}$	0.0049	1.22 (303 K)	46
$Ca_3(PO_4)_2$:Er/Yb	300–473	$^2H_{11/2} \rightarrow {}^4I_{15/2}/{}^4S_{3/2} \rightarrow {}^4I_{15/2}$	—	0.34 (300 K)	47
$Na_3Y(PO_4)_2$:Er/Yb	320–670	$^2H_{11/2} \rightarrow {}^4I_{15/2}/{}^4S_{3/2} \rightarrow {}^4I_{15/2}$	0.0027	1.1 (313 K)	48
$Na_3Y(PO_4)_2$:Er/Yb	320–670	$^4F_{9/2} \rightarrow {}^4I_{15/2}/{}^2H_{11/2} \rightarrow {}^4I_{15/2}$	0.16	0.8 (313 K)	48
$K_3Y(PO_4)_2$:Er/Yb	293–553	$^4F_{9/2} \rightarrow {}^4I_{15/2}/{}^2H_{11/2} \rightarrow {}^4I_{15/2}$	0.0044	0.86 (293 K)	49
$Sr_3(PO_4)_2$:Er/Yb	303–623	$^2H_{11/2} \rightarrow {}^4I_{15/2}/{}^4S_{3/2} \rightarrow {}^4I_{15/2}$	0.0070	0.88 (303 K)	50
$GdPO_4$:Er/Yb	293–673	$^2H_{11/2} \rightarrow {}^4I_{15/2}/{}^4S_{3/2} \rightarrow {}^4I_{15/2}$	—	0.74 (298 K)	51
$ZrSc(WO_4)_2PO_4$:Er/Yb	298–573	$^2H_{11/2} \rightarrow {}^4I_{15/2}/{}^4S_{3/2} \rightarrow {}^4I_{15/2}$	1.12	1.10 (298 K)	52
$Na_2SrP_2O_7$:Er/Yb	200–440	$^2H_{11/2} \rightarrow {}^4I_{15/2}/{}^4S_{3/2} \rightarrow {}^4I_{15/2}$	0.002	0.6 (240 K)	This work
$Na_2SrP_2O_7$:Er/Yb	200–440	$^2H_{11/2} \rightarrow {}^4I_{15/2}/{}^4F_{9/2} \rightarrow {}^4I_{15/2}$	0.0075	1.14 (200 K)	This work

decreasing gradually from 1.14% K^{-1} at 200 K to 0.28% K^{-1} at 440 K. All obtained values are listed in Table 2, along with the reported phosphates systems. As can be seen, the sensing sensitivity of our sample based on non-thermal coupled levels is relatively high, indicating that NSPO:Er,Yb is more suitable for temperature sensing applications.

Another important parameter related to temperature sensitivity is temperature uncertainty (δT).[51,52] This parameter indicates the smallest temperature change that can be detected. It depends on the performance of the system and experimental setup. δT can be determined by using the following equation:[53]

$$\delta T = \frac{1}{S_R}\frac{\partial \mathrm{LIR}}{\mathrm{LIR}},$$

where δLIR is the standard deviation of LIR data obtained from multiple measurements at a fixed temperature, while LIR represents the mean value obtained from these measurements. To evaluate the sensitivity of the detection system, we performed 20 LIR measurements on our sample at room temperature, as shown in the histograms in Fig. 9. The LIR uncertainty, defined as ∂LIR, was obtained from 20 measurements at 298 K.[54,55]

Fig. 10 shows the temperature uncertainty based on the LIR_{TCL} and LIR_{NTCL} of NSPO:Er, Yb at different temperatures. Based on the LIR_{TCL} method, the minimum temperature uncertainty obtained was about 1.31 K at 320 K; whereas based on the LIR_{NTCL} method, the minimum δT was 0.34 K at 200 K. Thus, it is clearly seen that the δT value of the optical thermometer obtained using the LIR_{NTCL} technique is lower than that obtained using the LIR_{TCL} technique.

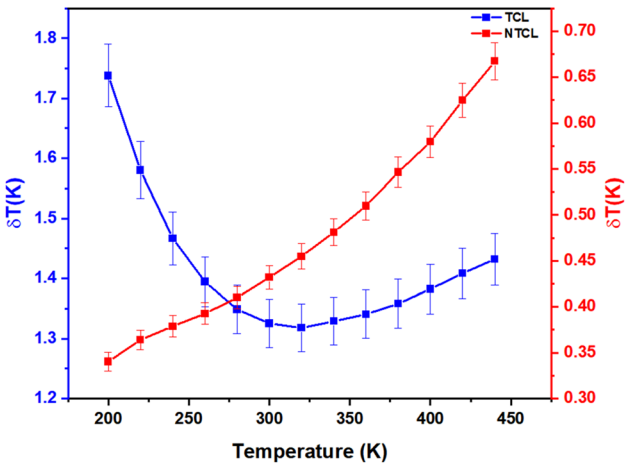

Fig. 10 Temperature uncertainty values δT of LIR_{TCL} and LIR_{NTCL}. The error bars indicate uncertainties due to experimental acquisition and data analysis.

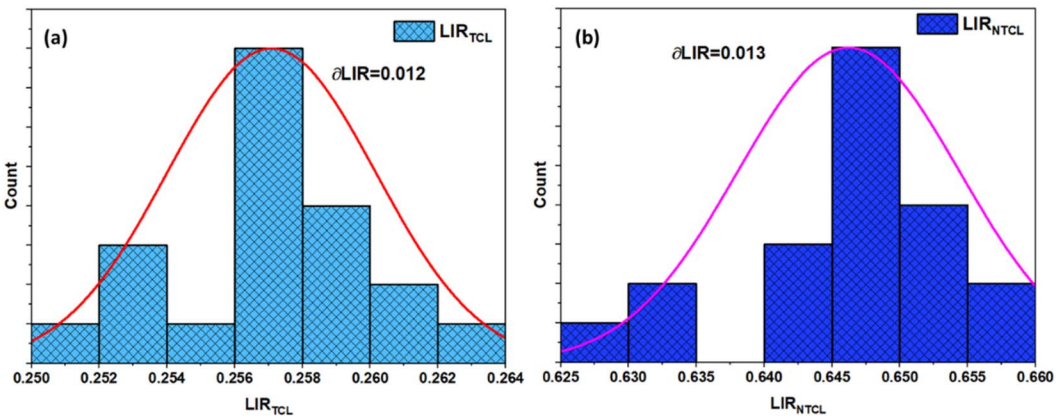

Fig. 9 Standard deviation obtained using 20 measurements at 298 K of (a) LIR_{TCL} and (b) LIR_{NTCL}.

4. Conclusions

In this study, we successfully synthesized $Na_2SrP_2O_7:Er^{3+}/Yb^{3+}$ phosphors *via* the solid-state method and explored their potential for optical thermometry in the 200–440 K temperature range under 980 nm excitation. The upconversion luminescence properties of these phosphors were thoroughly analyzed using the LIR method, considering both TCL and NTCL energy levels. The calculated maximum S_A and S_R values demonstrated that these materials exhibit strong temperature-dependent luminescence suitable for precise temperature sensing. Notably, the comparison between the LIR_{TCL} and LIR_{NTCL} methods revealed that the LIR_{NTCL} technique provides a lower minimum δT, reaching 0.34 K at 200 K, compared to 1.31 K at 320 K for the LIR_{TCL} technique. This indicates that the LIR_{NTCL} method offers superior resolution and accuracy for optical temperature sensing. Overall, the $Na_2SrP_2O_7:Er^{3+}/Yb^{3+}$ phosphors display excellent temperature sensitivity, high resolution, and versatility, making them highly promising candidates for advanced optical thermometry applications. These findings contribute to the development of more reliable and precise non-contact temperature sensing technologies, with potential applications in both scientific research and industrial environments.

Data availability

All data underlying the results are available as part of the article, and no additional source data are required.

Conflicts of interest

There are no conflicts to declare.

References

1 X. Wang, X. G. Kong, Y. Yu, Y. J. Sun and H. Zhang, *J. Phys. Chem. C*, 2007, **111**, 15119–15124.
2 N. Rakov and G. S. Maciel, *Dalton Trans.*, 2014, **43**, 16025–16030.
3 J. Zhang, J. Chen and Y. Zhang, *Inorg. Chem. Front.*, 2020, **7**, 4892–4901.
4 Y. Zi, Z. Yang, Z. Xu, X. Bai, A. Ullah, I. Khan, A. Ali Haider, J. Qiu, Z. Song, Y. Wang and Y. Cun, *J. Alloys Compd.*, 2021, **880**, 160156.
5 A. A. Kalinicheva, M. A. Kurochkina, A. Y. Kolomytseva, R. S. Khasbievab, E. Yu Kolesnikovc, E. Lähderantad and I. E. Kolesnikova, *Opt. Mater.*, 2019, **90**, 200–207.
6 X. Wang, O. S. Wolfbeis and R. J. Meier, *Chem. Soc. Rev.*, 2013, **42**, 7834–7869.
7 Y. Tu, S. Zhao, D. He, T. Wu, H. Zhang, R. Lei, L. Huang and S. Xu, *J. Mater. Chem.*, 2018, **6**, 7063–7069.
8 F. Vetrone, R. Naccache, A. Zamarrón, A. Juarranz de la Fuente, F. Sanz-Rodríguez, L. Martinez Maestro, E. Martín Rodriguez, D. Jaque, J. García Solé and J. A. Capobianco, *ACS Nano*, 2010, **4**, 3254–3258.
9 C. D. S. Brites, A. Millán and L. D. Carlos, *Handbook on the Physics and Chemistry of Rare Earths*, 2016, vol. 49, pp. 339–427.
10 C. Zaldo, *Lanthanide-Based Multifunctional Materials*, 2018, pp. 335–379.
11 M. Dramicanin, *Luminescence Thermometry: Methods, Materials, and Applications*, 2018.
12 D. Sevic, M. S. Rabasovic, M. G. Nikolic, J. Križan, S. Savic-Sevic and B. P. Marinkovic, *Opt. Quantum Electron.*, 2022, **54**, 523.
13 G. Bao, K. L. Wong, D. Jin and P. A. Tanner, *Light:Sci. Appl.*, 2018, **7**, 96.
14 Y. Cheng, Y. Gao, H. Lin, F. Huang and Y. Wang, *J. Mater. Chem.*, 2018, **6**, 7462–7478.
15 L. Xing, R. Ao, Y. Liu and W. Yang, Spectrochim, *Spectrochim. Acta, Part A*, 2019, **222**, 117159.
16 M. Ding, M. Zhang and C. Lu, *Mater. Lett.*, 2017, **209**, 52–55.
17 S. K. Ranjan, M. Mondal and V. K. Rai, *Mater. Res. Bull.*, 2018, **106**, 66–73.
18 J. Xing, F. Shang and G. Chen, *Ceram. Int.*, 2021, **47**, 8330–8337.
19 F. Ayachi, K. Saidi, W. Chaabani and M. Dammak, *J. Lumin.*, 2021, **240**, 118451.
20 K. Saidi, C. Hernández-Alvarez, M. Runowski, M. Dammak and I. R. Martín Benenzuela, *ACS Appl. Nano Mater.*, 2023, **6**, 19431–19442.
21 K. Saidi, I. Kachou, K. Soler-Carracedo, M. Dammak and I. R. Martín, *ACS Appl. Nano Mater.*, 2023, **6**, 17681–17690.
22 R. Bao, N. An, L. Ye and L. G. Wang, *Opt. Fiber Technol.*, 2019, **52**, 101989.
23 S. Li, W. Wang, X. Wei, L. Li, Q. Zhang, Y. Li and Y. Pan, *Opt. Mater.*, 2021, **113**, 110840.
24 Y. Li, W. Wang, Y. Pan, H. Chen, Q. Cao and X. Wei, *CrystEngComm*, 2020, **22**, 6302–6309.
25 L. Li, W. Wang, H. Chen, S. Li, Q. Zhang, Y. Pan and Y. Li, *J. Non-Cryst. Solids*, 2021, **573**, 121142.
26 L. Mukhopadhyay and V. Kumar Rai, *New J. Chem.*, 2017, **41**, 7650–7661.
27 A. K. Bedyal, V. Kumar and H. C. Swart, *J. Alloys Compd.*, 2020, **845**, 156352.
28 M. Fhoula, T. Koubaa and M. Dammak, *Opt. Laser Technol.*, 2020, **130**, 106352.
29 T. Chengaiah, C. K. Jayasankar, A. M. Babu and L. R. Moorthy, *Mater. Express*, 2014, **4**, 153–158.
30 W. Liu, X. Wang, Q. Zhu, X. Li, X. Sun and J. G. Li, *Sci. Technol. Adv. Mater.*, 2019, **20**, 949–963.
31 T. Zheng, L. Zhou, X. Qiu, D. Yang, M. Runowski, S. Lis, P. Du and L. Luo, *J. Lumin.*, 2020, **227**, 117517.
32 K. Saidi and M. Dammak, *J. Solid State Chem.*, 2021, **300**, 122214.
33 O. Ajili1, B. Louati1 and K. Guidara, *J. Mater. Sci.: Mater. Electron.*, 2018, **29**, 8649–8659.
34 O. Ajili, B. Louati and K. Guidara, *Indian J. Phys.*, 2018, **92**, 875–881.
35 C. Ming and M. Pei, *J. Mod. Opt.*, 2019, **66**, 1956–1960.
36 X. Cheng, X. Dong, K. Peng, H. Zhang, Y. Su and L. Jiang, *J. Electron. Mater.*, 2020, **49**, 518–523.

37 P. Gao, X. Li, Y. Gong, G. Shen, S. Zhang and L. Guan, *J. Rare Earths*, 2019, **37**, 937–942.
38 P. Singh, N. Jain, S. Shukla, A. Kumar Tiwari, K. Kumar, J. Singh and A. C. Pandey, *RSC Adv.*, 2023, **13**, 2939.
39 X. Huang, K. Huang, L. Chen, N. Chen, R. Lei, S. Zhao and S. Xua, *Opt. Mater.*, 2020, **107**, 110114.
40 S. A. Wade, S. F. Collins and G. W. Baxter, Fluorescence intensity ratio technique for optical fiber point temperature sensing, *J. Appl. Phys.*, 2003, **94**, 4743.
41 W. Xu, H. Zhao, Z. Zhang and W. Cao, *Sens. Actuators, B*, 2013, **178**, 520–524.
42 L. Li, Y. Zhou, F. Qin, Y. Zheng, H. Zhao and Z. Zhang, *Opt. Lett.*, 2017, **42**, 4837–4840.
43 X. Wang, J. Zheng, Y. Xuan and X. Yan, *Opt. Express*, 2013, **21**, 21596–21606.
44 Q. Han, H. Hao, J. Yang, Z. Sun, J. Sun, Y. Song, Y. Wang and X. Zhang, *J. Alloys Compd.*, 2019, **786**, 770–778.
45 I. Porosnicu, C. Colbea, F. Baiasu, M. Lungu, M. Cosmin Istrate, D. Avram and C. Tiseanu, *Methods Appl. Fluoresc.*, 2020, **8**, 035005.
46 Y. Chen, X. Y. Liu, G. H. Chen, T. Yang, C. L. Yuan, C. R. Zhou and J. W. Xu, *J. Mater. Sci.: Mater. Electron.*, 2017, **28**, 15657–15662.
47 K. M. Krishnaa, S. P. Tiwarib, A. Kumara and K. Kumar, *Sens. Actuators, A*, 2020, **315**, 112302.
48 P. Khajuria, A. K. Bedyal, M. Manhas, H. C. Swart, F. Durani and V. Kumar, *J. Alloys Compd.*, 2021, **877**, 160327.
49 J. Zhang, Y. Zhang and X. Jiang, *J. Alloys Compd.*, 2018, **748**, 438–445.
50 T. Zheng, L. Zhou, X. Qiu, D. Yang, M. Runowski, S. Lis and L. Luo, *J. Lumin.*, 2020, **227**, 117517.
51 S. Mohanty, J. García-Balduz, A. Alıcı, S. Premcheska, M. Lederer, A. Skirtach, K. Van Hecke and A. M. Kaczmarek, *ACS Appl. Mater. Interface*, 2024, **16**, 57580–57595.
52 J. Liao, Z. Han, F. Lin, B. Fu, G. Gong, H. Yan, H. Huang, H. R. Wen and B. Qiu, *Inorg. Chem.*, 2023, **62**, 9518–9527.
53 Z. Liu, Y. Li, X. Zhao, E. Y. B. Pun and H. Lin, *New J. Chem.*, 2023, **47**, 7263–7277.
54 J. F. C. B. Ramalho, S. F. H. Correia, L. S. Fu, L. L. F. António, C. D. S. Brites, P. S. André, R. A. S. Ferreira and L. D. Carlos, *Adv. Sci.*, 2019, **6**, 1900950.
55 K. Zhu, Z. Wang, H. Xu and Z. Fu, *Adv. Opt. Mater.*, 2022, **10**, 2201182.